PCCP

COMMUNICATION

View Article Online
View Journal

Cite this: DOI: 10.1039/c7cp00725f

Received 2nd February 2017,
Accepted 29th March 2017

DOI: 10.1039/c7cp00725f

rsc.li/pccp

Cage-like B_{39}^+ clusters with the bonding pattern of σ + π double delocalization: new members of the borospherene family†

Xiao-Yun Zhao,‡[a] Qiang Chen,‡[b] Hai-Ru Li,[a] Yue-Wen Mu,*[a] Hai-Gang Lu*[a] and Si-Dian Li*[a]

The recently observed cage-like borospherenes D_{2d} $B_{40}^{-/0}$ and C_3/C_2 B_{39}^- have attracted considerable attention in chemistry and materials science. Based on extensive global minimum searches and first-principles theory calculations, we present herein the possibility of cage-like C_s B_{39}^+ (1) and C_s B_{39}^+ (2) which possess five hexagonal and heptagonal faces and one filled hexagon and follow the bonding pattern of σ + π double delocalization with 12 delocalized π bonds over a σ-skeleton, adding two new members to the borospherene family. IR, Raman, and UV-vis spectra of C_s B_{39}^+ (1) and C_s B_{39}^+ (2) are computationally simulated to facilitate their experimental characterization.

Cage-like C_{60}, the first fullerene discovered in 1985,[1] pioneers the route to the currently popular carbon nanotubes[2] and graphenes.[3] However, only a few small free-standing fullerene-like clusters of other elements had been experimentally confirmed before 2014, including Au_{16}^-,[4] stannaspherene Sn_{12}^{2-},[5] and plumbaspherene Pb_{12}^{2-}.[6] As the lighter neighbor of carbon in the periodic table, boron is a typical electron-deficient element characterized with multicenter two-electron (mc-2e) bonds in both bulk allotropes and polyhedral molecules. The first all-boron fullerene B_{80} was theoretically proposed in 2007[7] by capping the 20 surface hexagons on the C_{60} motif. However, this beautiful I_h B_{80} cage was later found to be much less stable than its core–shell rivals at various theoretical levels.[8,9] In stark contrast to carbon clusters, small boron clusters $B_n^{-/0}$ have been experimentally confirmed to be planar or quasi-planar in an unprecedented wide range of sizes (n = 3–30, 35, 36),[10–25] unveiling a flat world of boron. Interestingly, small boron dihydride clusters $B_nH_2^{-/0}$ (n = 4–12) have proven to be elongated planar boron double-chains (BDCs) with two hydrogen terminals in both theory[26] and experiments,[27] strongly suggesting the importance of BDCs as building blocks in low-dimensional boron nanostructures. The first all-boron fullerenes D_{2d} $B_{40}^{-/0}$, dubbed borospherenes in the literature, were discovered in 2014 in a joint photoelectron spectroscopy (PES) and first-principles theory investigation,[28] paving the way to borospherene chemistry. Endohedral and exohedral $M@B_{40}$ (M = Ca, Sr) and $M\&B_{40}$ (M = Be, Mg) charge-transfer complexes were also predicted to be viably possible in experiments.[29] Shortly after $B_{40}^{-/0}$, the first axially chiral borospherenes C_3/C_2 B_{39}^- were observed in PES measurements in 2015[30] which may be further stabilized to form endohedral $Ca@B_{39}^+$.[31] In the past two years, our group has further expanded the borospherene family at the first-principles theory level to include the cage-like B_{41}^+/B_{42}^{2+},[32] B_{38}^{2-} (in $Ca@B_{38}$),[33] B_{37}^{3-} (in $Ca@B_{37}^-$),[34] and B_{36}^{4-} (in $Li_4\&B_{36}$)[35] clusters. These B_n^q borospherenes (n = 36–42, $q = n - 40$) are all composed of twelve interwoven BDCs with six hexagonal or heptagonal faces analogous to the well-known cube-like cubane (C_8H_8). They all follow the universal bonding pattern of σ + π double delocalization, with 12 multicenter two-electron π-bonds (12 mc-2e π) over a σ-skeleton made of n + 8 delocalized three-center-two-electron σ-bonds (n + 8 3c-2e σ).[28–35] Smaller seashell-like borospherenes B_{28}^- and B_{29}^- were later observed as minor isomers in PES experiments which also follow the σ + π double delocalization bonding pattern.[24,25] The discovery of the borospherene family effectively enriches the structural diversities of boron and has aroused considerable attention from chemists, physicists, and materials scientists.[36–42] A cage-like D_{2h} B_{38} was also recently proposed at the density functional theory (DFT) level.[43]

Based on extensive global minimum (GM) searches and first-principles theory calculations, we predict herein the existence of the cage-like C_s B_{39}^+ (**1**) and C_s B_{39}^+ (**2**) monocations which possess five hexagonal (n_6) and heptagonal (n_7) faces and one filled hexagon (n_6') on the cage surface with $n_6 + n_7 + n_6' = 6$ and follow the σ + π double delocalization bonding pattern with 12 delocalized π bonds over a σ-skeleton consisting of 46 delocalized σ bonds, adding two novel members to the borospherene family analogous to cubane (C_8H_8). B_{39}^+ (**1**) and B_{39}^+ (**2**) are the first borospherenes with a filled hexagon on the cage surface.

[a] Nanocluster Laboratory, Institute of Molecular Science, Shanxi University, Taiyuan 030006, China. E-mail: ywmu@sxu.edu.cn, luhg@sxu.edu.cn, lisidian@sxu.edu.cn
[b] Beijing National Laboratory for Molecular Sciences, State Key Laboratory for Structural Chemistry of Unstable and Stable Species, Institute of Chemistry, Chinese Academy of Sciences, Beijing 100190, China

† Electronic supplementary information (ESI) available. See DOI: 10.1039/c7cp00725f
‡ X. Y. Zhao and Q. Chen contributed equally to this work.

Extensive GM searches using both the Minima Hopping (MH)[44,45] and TGmin[18] algorithms were performed on B_{39}^+, in combination with manual structural constructions based on the previously reported planar, cage-like, and tubular isomers of B_{39}^- [30] and B_{38}^{2-}.[33] In total, more than 1700 stationary points were probed on the potential energy surface of B_{39}^+. Low-lying isomers were then fully optimized with frequencies checked at the DFT-PBE0 level[46] with the 6-311+G(d) basis set[47] using the Gaussian 09 suite.[48] The relative stabilities of the four lowest-lying isomers were further refined using the more accurate coupled cluster method with triple excitations (CCSD(T))[49–51] implemented in MOLPRO[52] with the 6-31G(d) basis set at the PBE0 geometries. The three lowest-lying isomers C_s B_{39}^+ (**1**), C_s B_{39}^+ (**2**), and C_s B_{39}^+ (**3**) obtained for B_{39}^+ are depicted in Fig. 1. More alternative low-lying isomers are summarized in Fig. S1 in the ESI.† The bonding patterns of the two lowest-lying C_s B_{39}^+ (**1**) and C_s B_{39}^+ (**2**) (Fig. 2) were analyzed with the adaptive natural density partitioning (AdNDP) approach.[53] Born–Oppenheimer molecular dynamics simulations were performed for C_s B_{39}^+ (**1**) at 300 K, 500 K, and 700 K for 30 ps (Fig. 3), using the software suite of CP2K.[54]

The cage-like B_{39}^+ (**1**) with the lowest vibrational frequency of 136 cm^{-1} at the PBE0 level turns out to be the global minimum of the monocation. It possesses two hexagons (n_6 = 2) in the front and at the back, three heptagons (n_7 = 3) on the top and two sides, and one filled hexagon (n_6' = 1) at the bottom with a hexacoordinate B at the center, in an overall symmetry of C_s. With six hexagonal and heptagonal faces in total including the filled hexagon (*i.e.* $n_6 + n_7 + n_6' = 6$), C_s B_{39}^+ (**1**) can also be approximately viewed as a distorted cubic box analogous to cubane, similar to other previously reported borospherenes.[28–35] It is mainly composed of interwoven BDCs except for the bottom area which contains a filled hexagon perpendicular to the molecular mirror. We notice that C_s B_{39}^+ (**1**) has the same geometry as the previously reported high-lying C_s B_{39}^- (**22**) monoanion[30] and can be obtained from the latter by detachment of two valence electrons. It follows Euler's rule, which in this case reads: E (90 edges) = F (47 triangular + 3 hexagonal + 3 heptagonal faces) + V (39 vertices) − 2. From another perspective, B_{39}^+ (**1**) can be built from eight nearly planar B_6 triangles (highlighted in gray in Fig. 1) at the corners

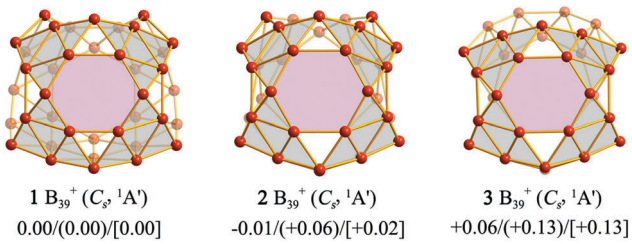

Fig. 1 Structures of the first three lowest-lying isomers of B_{39}^+ (**1**, **2**, and **3**) optimized at the PBE0/6-311+G(d) level, with the relative energies indicated in eV at the PBE0, TPSSh (in parentheses), and CCSD(T) (in square brackets) levels. The eight nearly planar B_6 triangles at the corners of the distorted cubic boxes and hexagonal faces in the front are highlighted in grey and pink, respectively.

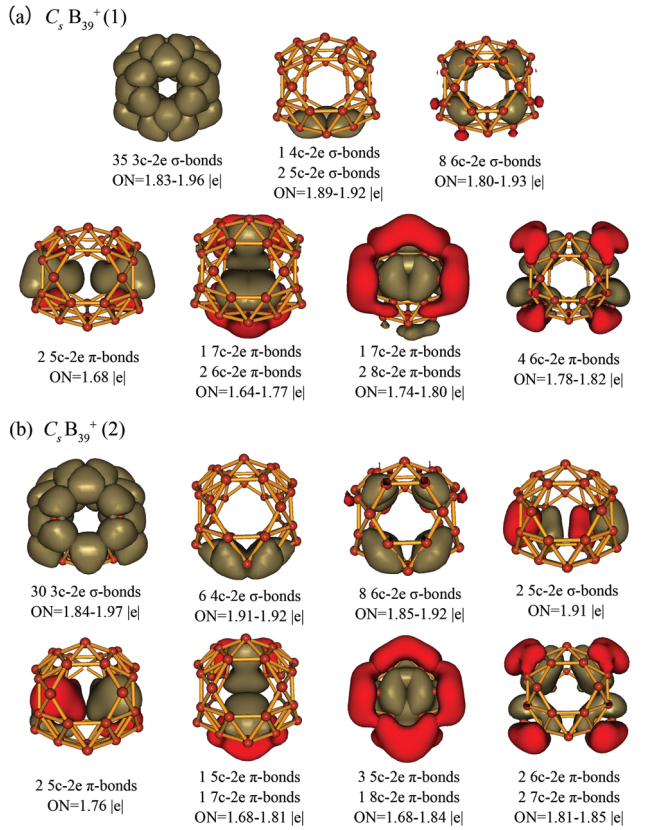

Fig. 2 AdNDP bonding patterns of (a) the global minimum C_s B_{39}^+ (**1**) and (b) the second lowest-lying C_s B_{39}^+ (**2**), with the occupation numbers (ONs) indicated.

of a distorted cube, similar to the situation in other reported borospherenes.[28–35]

The second lowest-lying cage-like C_s B_{39}^+ (**2**) with the lowest vibrational frequency of 141 cm^{-1} at PBE0 has one hexagon (n_6 = 1) in the front, four heptagons (n_7 = 4) on the top, back, and two sides, and one filled hexagon (n_6' = 1) at the bottom. It can also be viewed as a distorted cubic box with $n_6 + n_7 + n_6' = 6$. B_{39}^+ (**2**) has small relative energies of only −0.01, +0.06, and +0.02 eV with respect to B_{39}^+ (**1**) at the PBE0, TPSSh,[55] and CCSD(T) levels, respectively. Given the accuracies of the theoretical methods employed in this work, B_{39}^+ (**2**) and B_{39}^+ (**1**) can be viewed as practically iso-energetic isomers which are expected to coexist in experiments. We notice that B_{39}^+ (**2**) consists of two tetracoordinate "defect sites" on the waist at the back (Fig. 1), similar to the experimentally observed C_2 B_{39}^- (**2**) monoanion which has one tetracoordinate B atom on the waist.[30]

The third lowest-lying isomer C_s B_{39}^+ (**3**) which lies +0.13 eV higher than C_s B_{39}^+ (**1**) at the CCSD(T) level possesses three hexagons (n_6 = 3) in the front and two sides, two heptagons (n_7 = 2) on the top and back, and one filled hexagon (n_6' = 1) at the bottom, similar to C_s B_{39}^+ (**2**) (but with different numbers and orientations of hexagons and heptagons). It can be obtained from the previously reported C_s B_{38}^{2-} [33] by capping one hexagon at the bottom to form a filled hexagon. As shown

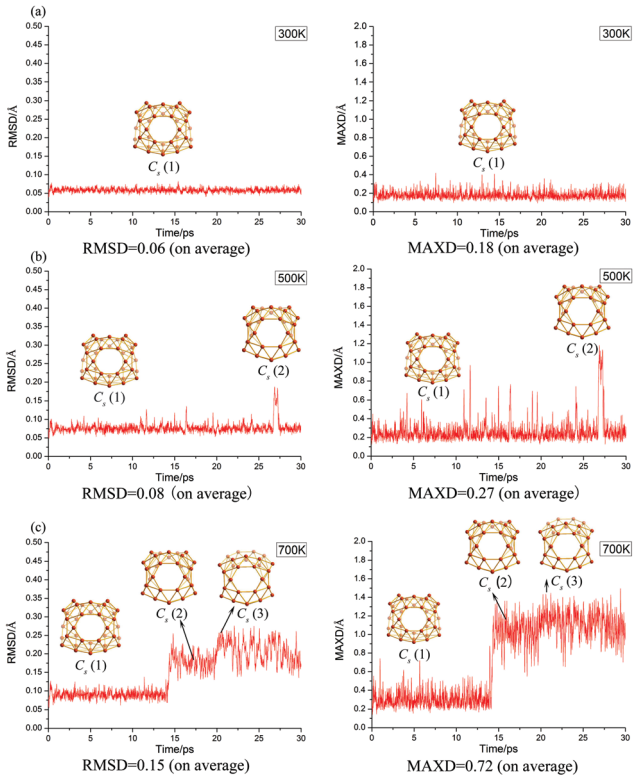

Fig. 3 Born–Oppenheimer molecular dynamics simulations of C_s B_{39}^+ (**1**) at (a) 300 K, (b) 500 K, and (c) 700 K, with the typical structures picked up during the simulations depicted. The root-mean-square-deviation (RMSD) and maximum bond length deviation (MAXD) values (on average) are indicated in Å.

in Fig. S1 (ESI†), the much concerned singlet triple-ring tubular C_{13} B_{39}^+ (**4**) turns out to be obviously less stable (0.24 eV) than B_{39}^+ (**1**) at the CCSD(T) level. The typical quasi-planar C_s B_{39}^+ (**8**) and C_s B_{39}^+ (**9**) have approximately the same relative energies of 0.31 eV at the PBE0/6-311+G(d) level. The axially chiral triplet C_3 B_{39}^+ (22) and singlet C_2 B_{39}^+ (32), which have the same geometry as the experimentally observed C_3 B_{39}^- and C_2 B_{39}^-,[30] have high relative energies of 0.67 eV and 0.90 eV, respectively. Other low-lying isomers all lie at least 0.30 eV higher than B_{39}^+ (**1**). We conclude that B_{39}^+ (**1**) and B_{39}^+ (**2**) as the global minima of the monocation and the all-boron analogs of cubane (C_8H_8) are the most possible isomers to be observed in experiments, while other high-lying isomers are unlikely to exist in thermodynamics.

The high stabilities of B_{39}^+ (**1**) and B_{39}^+ (**2**) originate from their unique bonding patterns, as shown in Fig. 2. Detailed AdNDP analyses indicate that B_{39}^+ (**1**) possesses 35 3c-2e σ bonds around the five hexagonal and heptagonal holes, 1 4c-2e and 2 5c-2e σ bonds at the bottom, and 8 6c-2e σ bonds at the eight corners of the distorted cubic box (Fig. 1) with occupation numbers (ONs) greater than 1.80 $|e|$. Over the σ skeleton, there exist 12 delocalized mc-2e π bonds (m = 5, 6, 7, 8) with ON > 1.64 $|e|$, with 2 5c-2e, 6 6c-2e, 2 7c-2e, and 2 8c-2e π bonds in an overall symmetry of C_s. B_{39}^+ (**1**) thus possesses a σ + π double delocalization, following the universal bonding pattern of the borospherene family.[28–35] Similarly, C_s B_{39}^+ (**2**) possesses 12 delocalized mc-2e π bonds over a σ-skeleton made of 46 delocalized σ bonds, again following the σ + π double delocalization bonding pattern. In particular, C_s B_{39}^+ (**2**) possesses 2 5c-2e π bonds and 2 5c-2e σ bonds over the two tetracoordinate B atoms on the waist at the back. In comparison with the experimentally observed C_3 B_{39}^- and C_2 B_{39}^- monoanions, which have 47 delocalized σ bonds and 12 delocalized π bonds,[30] both the C_s B_{39}^+ (**1**) and C_s B_{39}^+ (**2**) monocations with two less valence electrons possess 46 delocalized σ bonds and 12 delocalized π bonds. It is the unique filled hexagon with a hexacoordinate B center in B_{39}^+ (**1**) and B_{39}^+ (**2**) that generates the extra pair of π electrons to match the 12 delocalized π bonds required to form stable borospherenes in B_{39}^+. Such a bonding pattern imparts three-dimensional (3D) aromaticity to the cage-like clusters, as evidenced by the calculated nucleus independent chemical shift (NICS)[56] values of −40 ppm and −36 ppm at the cage centers of C_s B_{39}^+ (**1**) and C_s B_{39}^+ (**2**), respectively.

Extensive molecular dynamics (MD) simulations were performed on B_{39}^+ (**1**) to check its dynamical behaviors at various temperatures. As shown in Fig. 3, B_{39}^+ (**1**) is dynamically stable at room temperature (300 K), with root-mean-square-deviation and maximum bond length deviation values (on average) of RMSD = 0.06 Å and MAXD = 0.18 Å. However, at 500 K, it starts to hop between the two lowest-lying isomers C_s B_{39}^+ (**1**) and C_s B_{39}^+ (**2**) with RMSD = 0.08 Å and MAXD = 0.27 Å, with C_s B_{39}^+ (**1**) being the dominating isomer. Upon further increasing the temperature to 700 K, the system is found to fluctuate almost freely in concerted MXW mechanisms[57] among the three lowest-lying isomers C_s B_{39}^+ (**1**), C_s B_{39}^+ (**2**), and C_s B_{39}^+ (**3**) with RMSD = 0.15 Å and MAXD = 0.72 Å, resulting in B_{39}^+ nanobubbles hopping among the three almost equally distributed isomers (**1**, **2**, and **3**) in equilibrium states. Such dynamical behaviors appear to be similar to that of B_{39}^-,[57] B_{40},[37] and B_{40}^+.[58] The geometrical fluctuations in borospherenes[37,57,58] originate from their bonding fluctuations which guarantee further theoretical and experimental investigations.

Infrared photodissociation (IRPD) spectroscopy in combination with first-principles calculations has proven to be a powerful approach in the characterization of novel cluster monocations.[59,60] B_{39}^+ monocation was previously detected in the mass spectrum of B_n^+ clusters (n = 2–52).[61] It is therefore possible to measure its IRPD spectrum in gas phases by optimizing the experimental conditions. To facilitate future experiments, we computationally simulate the IR spectra of both C_s B_{39}^+ (**1**) and C_s B_{39}^+ (**2**) in Fig. 4a and compare them with that of the high-symmetry borospherene monocation D_{2d} B_{40}^+.[58] The IR spectra of the three cage-like monocations exhibit obvious similarities with the major IR peaks lying between 900 and 1400 cm^{-1}, though the spectra of B_{39}^+ (**1**) and C_s B_{39}^+ (**2**) are much more complicated due to their low geometrical symmetries. There exist four strong IR peaks at 1257 cm^{-1} (a′), 1122 (a′), 1055 cm^{-1} (a′), and 963 cm^{-1} (a′) for C_s B_{39}^+ (**1**) and at 1337 cm^{-1} (a′), 1224 cm^{-1} (a′), 1082 cm^{-1} (a′), and 975 cm^{-1} (a″) for C_s B_{39}^+ (**2**) which may serve as finger prints to characterize these lowest-lying isomers.

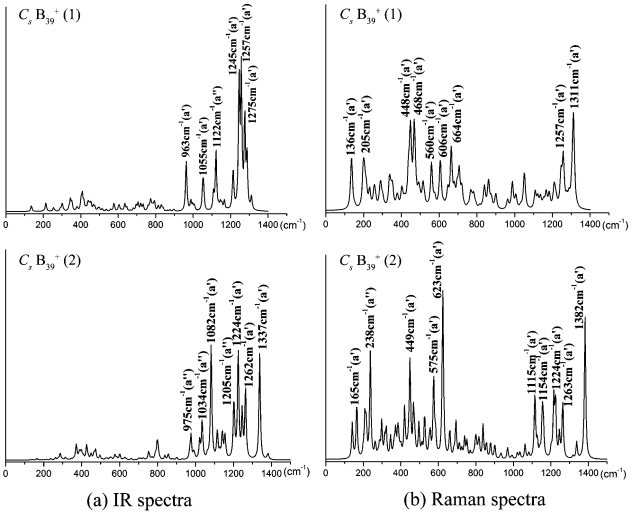

Fig. 4 Simulated IR and Raman spectra of C_s B_{39}^+ (**1**) and C_s B_{39}^+ (**2**) at the PBE0/6-311+G(d) level.

The strong Raman peaks of C_s B_{39}^+ (**1**) and C_s B_{39}^+ (**2**) (Fig. 4b) exhibit clear red-shifts with respect to that of D_{2d} B_{40}^+.[58] The major Raman peaks occur at 1311 cm^{-1} (a′), 1257 cm^{-1} (a′), 448 cm^{-1} (a′), 205 cm^{-1} (a′), and 136 cm^{-1} (a′) for C_s B_{39}^+ (**1**) and 1382 cm^{-1} (a′), 1224 cm^{-1} (a′), 623 cm^{-1} (a′), 449 cm^{-1} (a′), 238 cm^{-1} (a″), and 165 cm^{-1} (a′) for C_s B_{39}^+ (**2**). Detailed vibrational analyses indicate that the vibrations at 205 cm^{-1} (a′) and 136 cm^{-1} (a′) in C_s B_{39}^+ (**1**) and at 238 cm^{-1} (a′) and 165 cm^{-1} (a′) in C_s B_{39}^+ (**2**) represent typical radial breathing modes (RBMs) of the two isomers. An intensive RBM peak at 210 cm^{-1} was used to characterize the hollow structures in single-walled boron nanotubes.[62] The IR and Raman spectra of C_s B_{39}^+ (**3**) are simulated in Fig. S3 (ESI†) for comparison.

Finally, we simulate the UV-vis spectra of C_s B_{39}^+ (**1**) and C_s B_{39}^+ (**2**) using the TD-DFT approach[63] at the PBE0 level (Fig. 5) and compare them with that of D_{2d} B_{40}^+.[58] These borospherene monocations exhibit certain similarities in their UV spectra, with strong absorption peaks occurring at 211 nm, 242 nm, 280 nm, 304 nm, and 412 nm for C_s B_{39}^+ (**1**) and 219 nm, 259 nm, 299 nm, 338 nm, and 352 nm for C_s B_{39}^+ (**2**). These UV features originate from electron transitions from the deep inner shells to the high-lying unoccupied molecular orbitals of the monocations. The weak absorptions above 500 nm involve electron transitions from the highest and second highest occupied molecular orbitals (HOMO and HOMO−1) of the systems.

In summary, based on extensive GM searches and first-principles theory calculations, we have presented the possibility of the cage-like B_{39}^+ (**1**) and B_{39}^+ (**2**) borospherene monocations which, as the well-defined global minima of the system, possess five hexagonal and heptagonal faces and one filled hexagon on the cage surface. Detailed orbital analyses indicate that these borospherenes possess 3D aromaticity and follow the universal bonding pattern of σ + π double delocalization. The unique filled hexagon on the cage surface of C_s B_{39}^+ (**1**) and C_s B_{39}^+ (**2**) plays a key role in the formation of the 12 delocalized π bonds required to form stable borospherene monocations with less than 40 boron atoms. Their IR, Raman, and UV-vis spectra have been computationally simulated to facilitate their spectral characterization. Cubic-box-like borospherene neutrals or cations with more than one filled hexagons or heptagons may also be possible.

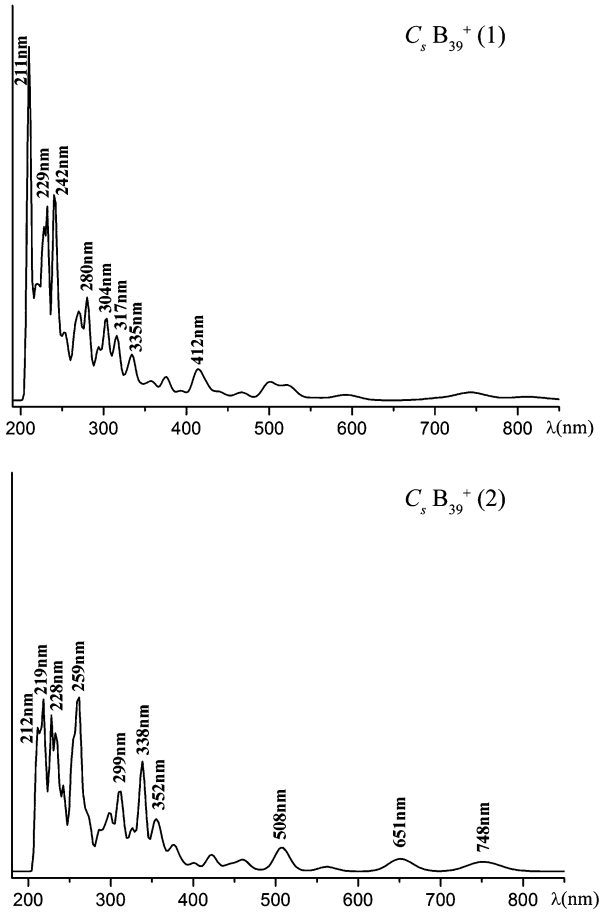

Fig. 5 Simulated UV-vis absorption spectra of C_s B_{39}^+ (**1**) and C_s B_{39}^+ (**2**) at the PBE0/6-311+G(d) level.

Acknowledgements

The project was financially supported by the National Natural Science Foundation of China (21373130).

Notes and references

1 H. W. Kroto, J. R. Heath, S. C. O'Brien, R. F. Curl and R. E. Smalley, *Nature*, 1985, **318**, 162–163.
2 M. Monthioux and V. L. Kuznetsov, *Carbon*, 2006, **44**, 1621–1623.
3 K. S. Novoselov, A. K. Geim, S. V. Morozov, D. Jiang, Y. Zhang, S. V. Dubonos, I. V. Grigorieva and A. A. Firsov, *Science*, 2004, **306**, 666–669.
4 S. Bulusu, X. Li, L. S. Wang and X. C. Zeng, *Proc. Natl. Acad. Sci. U. S. A.*, 2006, **103**, 8326–8330.

5 L. F. Cui, X. Huang, L. M. Wang, D. Y. Zubarev, A. I. Boldyrev, J. Li and L. S. Wang, *J. Am. Chem. Soc.*, 2006, **128**, 8390–8391.
6 L. F. Cui, X. Huang, L. M. Wang, J. Li and L. S. Wang, *J. Phys. Chem. A*, 2006, **110**, 10169–10172.
7 N. G. Szwacki, A. Sadrzadeh and B. I. Yakobson, *Phys. Rev. Lett.*, 2007, **98**, 166804.
8 F. Y. Li, P. Jin, D. E. Jiang, L. Wang, S. B. Zhang, J. J. Zhao and Z. F. Chen, *J. Chem. Phys.*, 2012, **136**, 074302.
9 S. Goedecker, W. Hellmann and T. Lenosky, *Phys. Rev. Lett.*, 2005, **95**, 055501.
10 H. J. Zhai, A. N. Alexandrova, K. A. Birch, A. I. Boldyrev and L. S. Wang, *Angew. Chem., Int. Ed.*, 2003, **42**, 6004.
11 H. J. Zhai, B. Kiran, J. Li and L. S. Wang, *Nat. Mater.*, 2003, **2**, 827–833.
12 B. Kiran, S. Bulusu, H. J. Zhai, S. Yoo, X. C. Zeng and L. S. Wang, *Proc. Natl. Acad. Sci. U. S. A.*, 2005, **102**, 961–964.
13 A. P. Sergeeva, Z. A. Piazza, C. Romanescu, W. L. Li, A. I. Boldyrev and L. S. Wang, *J. Am. Chem. Soc.*, 2012, **134**, 18065–18073.
14 W. Huang, A. P. Sergeeva, H. J. Zhai, B. B. Averkiev, L. S. Wang and A. I. Boldyrev, *Nat. Chem.*, 2010, **2**, 202–206.
15 I. A. Popov, Z. A. Piazza, W. L. Li, L. S. Wang and A. I. Boldyrev, *J. Chem. Phys.*, 2013, **139**, 144307.
16 E. Oger, N. R. M. Crawford, R. Kelting, P. Weis, M. M. Kappes and R. Ahlrichs, *Angew. Chem., Int. Ed.*, 2007, **46**, 8503–8506.
17 W. L. Li, Y. F. Zhao, H. S. Hu, J. Li and L. S. Wang, *Angew. Chem., Int. Ed.*, 2014, **53**, 5540–5545.
18 Z. A. Piazza, H. S. Hu, W. L. Li, Y. F. Zhao, J. Li and L. S. Wang, *Nat. Commun.*, 2014, **5**, 3113.
19 A. P. Sergeeva, I. A. Popov, Z. A. Piazza, W. L. Li, C. Romanescu, L. S. Wang and A. I. Boldyrev, *Acc. Chem. Res*, 2014, **47**, 1349–1358.
20 W. L. Li, Q. Chen, W. J. Tian, H. Bai, Y. F. Zhao, H. S. Hu, J. Li, H. J. Zhai, S. D. Li and L. S. Wang, *J. Am. Chem. Soc.*, 2014, **136**, 12257–12260.
21 Q. Chen, G. F. Wei, W. J. Tian, H. Bai, Z. P. Liu, H. J. Zhai and S. D. Li, *Phys. Chem. Chem. Phys.*, 2014, **16**, 18282–18287.
22 X. M. Luo, T. Jian, L. J. Cheng, W. L. Li, Q. Chen, R. Li, H. J. Zhai, S. D. Li, A. I. Boldyrev, J. Li and L. S. Wang, *Chem. Phys. Lett.*, 2017, DOI: 10.1016/j.cplett.2016.12.051.
23 W. L. Li, R. Pal, Z. A. Piazza, X. C. Zeng and L. S. Wang, *J. Chem. Phys.*, 2015, **142**, 204305.
24 Y. J. Wang, Y. F. Zhao, W. L. Li, T. Jian, Q. Chen, X. R. You, T. Ou, X. Y. Zhao, H. J. Zhai, S. D. Li, J. Li and L. S. Wang, *J. Chem. Phys.*, 2016, **144**, 064307.
25 H. R. Li, T. Jian, W. L. Li, Ch. Q. Miao, Y. J. Wang, Q. Chen, X. M. Luo, K. Wang, H. J. Zhai, S. D. Li and L. S. Wang, *Phys. Chem. Chem. Phys.*, 2016, **18**, 29147–29155.
26 D. Z. Li, Q. Chen, Y. B. Wu, H. G. Lu and S. D. Li, *Phys. Chem. Chem. Phys.*, 2012, **14**, 14769–14774.
27 W. L. Li, C. Romanescu, T. Jian and L. S. Wang, *J. Am. Chem. Soc.*, 2012, **134**, 13228–13231.
28 H. J. Zhai, Y. F. Zhao, W. L. Li, Q. Chen, H. Bai, H. S. Hu, Z. A. Piazza, W. J. Tian, H. G. Lu, Y. B. Wu, Y. W. Mu, G. F. Wei, Z. P. Liu, J. Li, S. D. Li and L. S. Wang, *Nat. Chem.*, 2014, **6**, 727–731.
29 H. Bai, Q. Chen, H. J. Zhai and S. D. Li, *Angew. Chem., Int. Ed.*, 2015, **54**, 941–945.
30 Q. Chen, W. L. Li, Y. F. Zhao, S. Y. Zhang, H. S. Hu, H. Bai, H. R. Li, W. J. Tian, H. G. Lu, H. J. Zhai, S. D. Li, J. Li and L. S. Wang, *ACS Nano*, 2015, **9**, 754–760.
31 Q. Chen, T. Gao, W. J. Tian, H. Bai, S. Y. Zhang, H. R. Li, C. Q. Miao, Y. W. Mu, H. G. Lu, H. J. Zhai and S. D. Li, *Phys. Chem. Chem. Phys.*, 2015, **17**, 19690–19694.
32 Q. Chen, S. Y. Zhang, H. Bai, W. J. Tian, T. Gao, H. R. Li, C. Q. Miao, Y. W. Mu, H. G. Lu, H. J. Zhai and S. D. Li, *Angew. Chem., Int. Ed.*, 2015, **54**, 8160–8164.
33 Q. Chen, H. R. Li, Ch. Q. Miao, Y. J. Wang, H. G. Lu, Y. W. Mu, G. M. Ren, H. J. Zhai and S. D. Li, *Phys. Chem. Chem. Phys.*, 2016, **18**, 11610–11615.
34 Q. Chen, H. R. Li, W. J. Tian, H. G. Lu, H. J. Zhai and S. D. Li, *Phys. Chem. Chem. Phys.*, 2016, **18**, 14186–14190.
35 W. J. Tian, Q. Chen, H. R. Li, M. Yan, Y. W. Mu, H. G. Lu, H. J. Zhai and S. D. Li, *Phys. Chem. Chem. Phys.*, 2016, **18**, 9922–9926.
36 R. X. He and X. C. Zeng, *Chem. Commun.*, 2015, **51**, 3185–3188.
37 G. Martínez-Guajardo, J. L. Cabellos, A. Díaz-Celaya, S. Pan, R. Islas, P. K. Chattaraj, T. Heine and G. Merino, *Sci. Rep.*, 2015, **5**, 11287.
38 W. Wang, Y. D. Guo and X. H. Yan, *RSC Adv.*, 2016, **6**, 40155–40161.
39 G. P. Gao, F. X. Ma, Y. L. Jiao, Q. Sun, Y. Jiao, E. Waclawik and A. Du, *Comput. Mater. Sci.*, 2015, **108**, 38–41.
40 Z. Yang, Y. L. Ji, G. Q. Lan, L. C. Xu, X. G. Liu and B. Xu, *Solid State Commun.*, 2015, **217**, 38–42.
41 Y. Yang, Z. H. Zhang, E. S. Penev and B. I. Yakobson, *Nanoscale*, 2017, **9**, 1805–1810.
42 H. Bai, B. Bing, L. Zhang, W. Huang, Y. W. Mu, H. J. Zhai and S. D. Li, *Sci. Rep.*, 2016, **6**, 35518.
43 J. Lv, Y. Wang, L. Zhu and Y. Ma, *Nanoscale*, 2014, **6**, 11692–11696.
44 S. De, A. Willand, M. Amsler, P. Pochet, L. Genovese and S. Goedecker, *Phys. Rev. Lett.*, 2011, **106**, 225502.
45 S. Goedecker, W. Hellmann and T. Lenosky, *Phys. Rev. Lett.*, 2005, **95**, 055501.
46 C. Adamo and V. Barone, *J. Chem. Phys.*, 1999, **110**, 6158.
47 R. Krishnan, J. S. Binkley, R. Seeger and J. A. Pople, *J. Chem. Phys.*, 1980, **72**, 650–654.
48 M. J. Frisch, *et al.*, *Gaussian 09, Revision A.2*, Gaussian Inc., Wallingford, CT, 2009.
49 J. Čižek, *Adv. Chem. Phys.*, 1969, **14**, 35.
50 G. D. Purvis and R. J. Bartlett, *J. Chem. Phys.*, 1982, **76**, 1910.
51 K. Raghavachari, G. W. Trucks, J. A. Pople and M. Head-Gordon, *Chem. Phys. Lett.*, 1989, **157**, 479.
52 (*a*) H. J. Werner, P. J. Knowles, G. Knizia, F. R. Manby and M. Schütz, *Wiley Interdiscip. Rev.: Comput. Mol. Sci.*, 2012, **2**, 242–253; (*b*) H. J. Werner, P. J. Knowles, G. Knizia, F. R. Manby, M. Schütz, *et al.*, MOLPRO, version 2012.1, http://www.molpro.net.
53 D. Yu. Zubarev and A. I. Boldyrev, *Phys. Chem. Chem. Phys.*, 2008, **10**, 5207.

54 J. VandeVondele, M. Krack, F. Mohamed, M. Parrinello, T. Chassaing and J. Hutter, *Comput. Phys. Commun.*, 2005, **167**, 103.
55 J. Tao, J. P. Perdew, V. N. Staroverov and G. E. Scuseria, *Phys. Rev. Lett.*, 2003, **91**, 146401.
56 P. v. R. Schleyer and C. Maerker, *J. Am. Chem. Soc.*, 1996, **118**, 6317–6318.
57 T. T. Gao, Q. Chen, Y. W. Mu, H. G. Lu and S. D. Li, *AIP Adv.*, 2016, **6**, 065110.
58 H. R. Li, Q. Chen, X. X. Tian, H. G. Lu, H. J. Zhai and S. D. Li, *J. Mol. Model.*, 2016, **22**, 124.
59 G. J. Wang, M. F. Zhou, J. T. Goettel, G. J. Schrobilgen, J. Su, J. Li, T. Schloder and S. Riedel, *Nature*, 2014, **514**, 475–477.
60 M. R. Fagiani, X. W. Song, P. Petkov, S. Debnath, S. Gewinner, W. Schöllkopf, T. Heine, A. Fielicke and K. R. Asmis, *Angew. Chem., Int. Ed.*, 2017, **56**, 501–504.
61 S. J. L. Placa, P. A. Roland and J. J. Wynne, *Chem. Phys. Lett.*, 1992, **190**, 163–168.
62 D. Ciuparu, R. F. Klie, Y. M. Zhu and L. Pfefferle, *J. Phys. Chem. B*, 2004, **108**, 3967–3969.
63 R. Bauernschmitt and R. Ahlrichs, *Chem. Phys. Lett.*, 1996, **256**, 454–464.

